




Study on Stick-slip Instability and Directionality on Bimaterial Faults

Ao Lei*

School of Civil Engineering, Chongqing University, Chongqing 400045, P. R. China
rio_0v0@163.com

Abstract: Earthquakes have significant impacts on the environment and society. Most tectonic earthquakes result from relative sliding due to faults' frictional instability. Among these, bimaterial faults, where different materials limit the fault interface, commonly exhibit rapid and unpredictable sticky sliding instability, leading to high levels of destruction. The asymmetric stress distribution in bimaterial fault systems results in complex failure modes, underscoring the significance of studying their failure mechanisms. This study, based on rock shear sliding experiments, explores the influence of bimaterial fault stick-slip instability by varying normal stress and shear loading rates to simulate ground stress and fault movement. Findings reveal an uneven stress field distribution during sticky slip instability, with a non-linear positive correlation between normal stress levels and stress drop between faults. Increasing normal stress enhances sliding weakening displacement. The directionality of rupture propagation during instability pertains to varied rupture modes and velocities across different directions. Notably, a critical transitional normal stress and loading rate exist between sticky sliding failure and smooth failure behavior.

Keywords: Sticky-slip, Bimaterial Fault, Shear Sliding; Rupture Propagation; Rupture Mode.

1 Introduction

Shallow tectonic earthquakes are renowned for their suddenness, potent destructive force, and extensive damage, inflicting substantial human, material, and economic losses globally. These earthquakes stem from the instantaneous instability of faults^[1], with research indicating that stick-slip instability due to fault displacement is the primary driver of shallow structural earthquakes^[2-4]. Byerlee proposed a spring slider model in 1978 to explain the phenomenon of stickiness^[5]. Afterwards, Dietrich and Runia introduced the velocity-state friction constitutive relationship^[6]. The study of frictional slip at homogeneous fault interfaces has advanced significantly in understanding fracture propagation characteristics. The Rosakis team conducted experimental research on pre-cracked organic glass panels (PMMA) and discovered that the destructive force of ultra-shear earthquakes is significantly greater than that of typical low-speed earthquakes^[7,8]. In their study on stick-slip of dissimilar materials,

© The Author(s) 2025

W. Guo et al. (eds.), *Proceedings of the 3rd International Conference on Green Building, Civil Engineering and Smart City (GBCESC 2024)*, Advances in Engineering Research 264,

https://doi.org/10.2991/978-94-6463-728-1_3

where the interface on both sides of the fault is constrained by different materials, Shlomain et al. discovered that dissimilar materials exhibit unique coupling properties and identified a new fracture mode named "slip pulse"^[9-11]. Xia et al. examined the impact of low-speed zones on earthquake rupture and observed the directional characteristics of rupture velocity and rupture mode^[12].

However, most of the studies mentioned above are focused on stick-slip instability at the interface of homogeneous materials, using materials like PMMA, PC, etc., rather than real rock materials. There is a lack of research on stick-slip instability in real rock masses using dual materials. Therefore, this study employs real rock stick-slip experiments to delve into the coupling characteristics, fracture modes, and directional aspects of fracture propagation in bimaterials, unveiling the mechanism of bimaterial fault stick-slip instability. This research aids in understanding the fundamental nature and mechanisms of earthquakes, providing a crucial foundation for determining seismic characteristics such as the location, depth, and type of earthquake sources, and enhancing the accuracy and reliability of earthquake warning systems.

2 Experimental System

2.1 Material properties

The simulated fault system employed in our study comprises an upper block of basalt and a lower block of granite. These constituent specimens, sourced from a quarry in Haikou city, Hainan Province, exhibit the fundamental physical properties displayed in Table 1.

Table 1. Basic parameters of sample

Material	Dimension (mm)	Young's modulus E(GPa)	Shear wave velocity v_s (km/s)	Poisson ratio μ	Density ρ (kg/m ³)
Basalt	180 × 110 × 20	61	2.71	0.25	2690
Granite	220 × 110 × 20	52	3.32	0.27	2662

This experiment adopts a biaxial shear experimental model, which ensures the implementation of large slip displacement, fault interface monitoring, unchanged contact area during the shear process, and simple operation. The horizontal movement of the upper block is limited by a higher stiffness pressure head, which tightly connects the upper block to the pressure head, so that when the device slips, the upper block will not bounce off the pressure head. The lower block is placed on a device with both bottom and left rigid blocks, and the bottom rigid block is installed on a roller bearing. When shear force is applied, the lower block can overcome frictional resistance and slide relatively freely in that direction, achieving almost no frictional resistance between the slider and the supporting platform, as shown in Fig. 1.

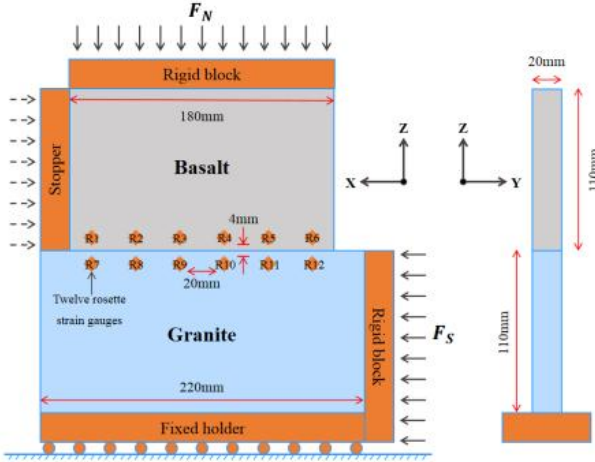


Fig. 1. Schematic diagram of experimental system.

2.2 Loading configuration

In this study, we employed the WDAJ-600 microcomputer-controlled electro-hydraulic servo rock shear rheology testing machine to load the device. To maintain consistency in surface roughness, all specimens were abraded using identical silicon carbide sandpaper.

The axial positive stress (F_n) is loaded to a predetermined value (2MPa, 3MPa, 4MPa) by "stress control". The shear force (F_s) is loaded by "displacement control". At each predetermined value, the shear loading rate is set to 0.1, 0.2, 0.4 mm/min for loading until sliding occurs. It is worth noting that the positive stress is set as a small value of 0.1MPa (non-experimental preset value), mainly to eliminate a series of errors caused by uneven and uneven force on the upper contact surface. For further information on the measurement method that employs a high-precision, multi-channel strain acquisition system, please consult the work of Zhou's team^[13].

3 Results

3.1 Stress variation law of bimaterial stick-slip instability

From Fig. 2a and b, it can be seen that with the progress of shear loading, there is a significant periodic fluctuation in stress. The process of stress gradually increasing and then suddenly decreasing is called a sticky slip event, which corresponds to the accumulation and release of strain energy, respectively. When dynamic rupture penetrates the entire interface, the overall movement of the fault will lead to significant stress weakening, an increase in relative slip, and the occurrence of slip. This phenomenon is called slip weakening. This periodic phenomenon of stress is due to the fact that at the moment of stick slip, the microscopic discrete contact points of the upper and lower blocks of the fault will experience a very brief "detachment".

Once the stick slip stops, the upper and lower discrete contact points will recombine. At this point, the stress will gradually return to its original value, and the magnitude of the earthquake is related to the amplitude of stress fluctuations (stress drop $\Delta\sigma$). According to Fig. 2c, at the same shear rate, the shear stress drop increases with the increase of normal stress, showing a non-linear positive correlation. Under the same normal stress, the shear stress drop decreases with the increase of shear velocity, and the time interval between occurrence of stick slip events also decreases, that is, they occur more frequently. Finally, the sliding mode between faults will gradually transition from stick slip to stable sliding mode.

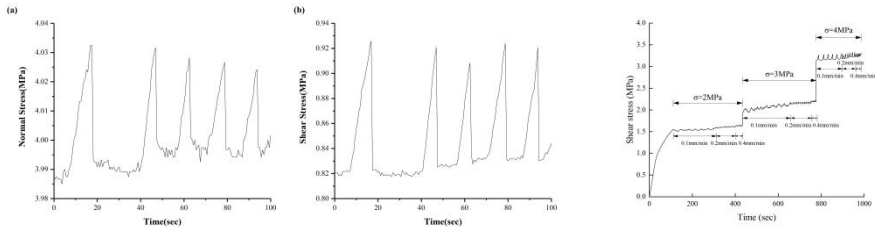


Fig. 2. Load stress-time relationship curve.(a) Load normal stress-time curve; (b) Load shear stress-time curve; (c) Shear stress-time curves under different normal stresses and shear rates.

We use the "nucleation point" to measure the location of the rupture, because compared to other points, points with higher ratios of normal and shear stresses are often more likely to become "breakthrough points", that is, the site where the sticky slip event nucleates and nurtures. Through Fig. 3, it is found that the distribution of normal stress and shear stress along the fault plane in the upper and lower test blocks is non-uniform. This non-uniformity is mainly caused by the uneven distribution of contact areas at discrete contact points between faults. Different contact areas at different positions will lead to different stress levels at corresponding positions. Secondly, the maximum stress ratio occurs at both ends, forming two potential nucleation points near R1 ($X=35\text{mm}$) and R6 ($X=185\text{mm}$). The main reason is that closer to the fixed end (loading end), the greater the constraint, resulting in stress concentration. We can more clearly reflect the time and sequence of local point failure by observing the time and sequence of the peak shear stress, as shown in Fig. 4. It can be seen that there is a chronological order of the time when the shear stress reaches its peak at each point along the fault plane, revealing that the stick-slip instability is destroyed from point to surface, belonging to type II fracture. That is, the initiation point on the section gradually expands to form multiple nucleation zones, which are interconnected and ultimately lead to the instability of the entire section. The stress drop time at point R1 in basalt lags behind that at point R7 in granite, exhibiting bimaterial asymmetry, with softer materials often fracturing earlier than harder materials.

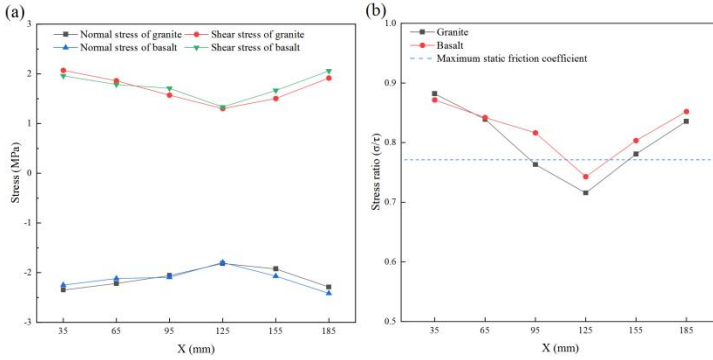


Fig. 3. Distribution of stress and stress ratio along the fault plane under normal stress of 2MPa.(a) Stress distribution along the fault plane (X is the distance from the shear loading end) ; (b) Distribution of stress ratio (σ/τ).

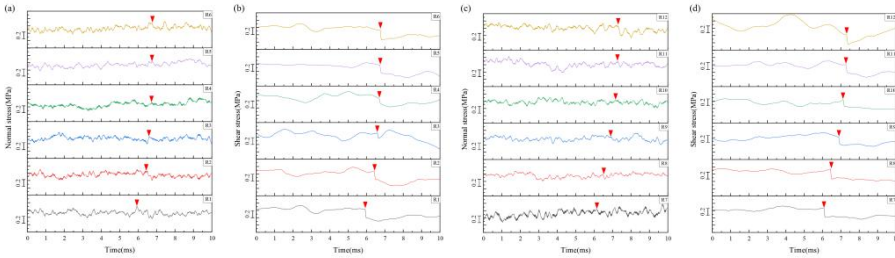


Fig. 4. Stress-time curves at each measuring point of the upper and lower specimens (normal stress of 2MPa, shear rate of 0.1mm/min). (a) The normal stress curve of basalt; (b) Shear stress curve of basalt; (c) Granite normal stress curve; (d) Shear stress curve of granite. (The time variation curves before the peak shear stress and after the shear stress drop were smoothed. The red triangle symbol represents the moment when the stress reaches its peak.)

3.2 Displacement variation law of bimaterial stick-slip instability

As shown in Fig. 5, the increase in displacement also exhibits periodic characteristics, and one of the stick slip events is divided into three main periods. They are respectively the interseismic viscous period (displacement remains basically unchanged), the precursor slip period (displacement slowly increases), and the coseismic slip period (displacement rapidly increases). The precursor slip, co seismic slip, and total slip all increase with the increase of normal stress. As the shear rate increases, the precursor slip and co seismic slip show a decreasing trend.

In Fig. 6, it is evident that certain points are the first to undergo damage, leading to relative displacement. As time progresses, the strain gauges will fail, causing the curve to straighten. With the increase in axial load, slip no longer propagates sequentially along the fault measuring point at 3MPa; instead, two nucleation points emerge at both ends, initiating fracture propagation in two directions along the fault.

Furthermore, the duration of the precursor slip period has notably extended. This extension is attributed to the rise in axial pressure, the reinforcement of constraint forces on the fault plane, and the accumulation of strain energy on the fault, ultimately influencing the overall sliding time.

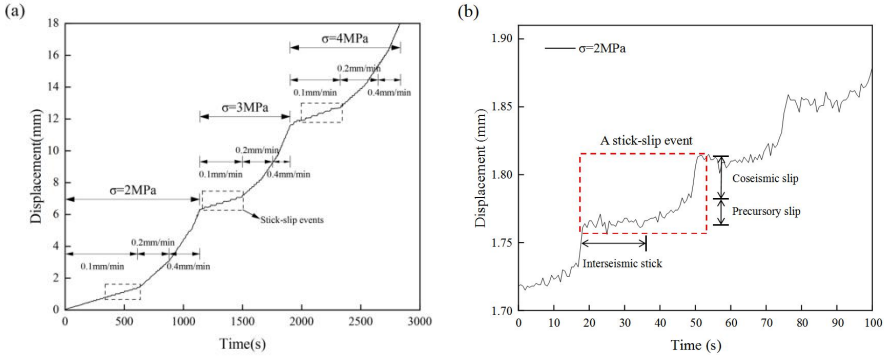


Fig. 5. Sticky-slip instability displacement time graph. (a) Displacement time graph under different normal stresses and shear rates; (b) Enlarged image of stick-slip instability event. (The red rectangular box represents a complete stick slip event.)

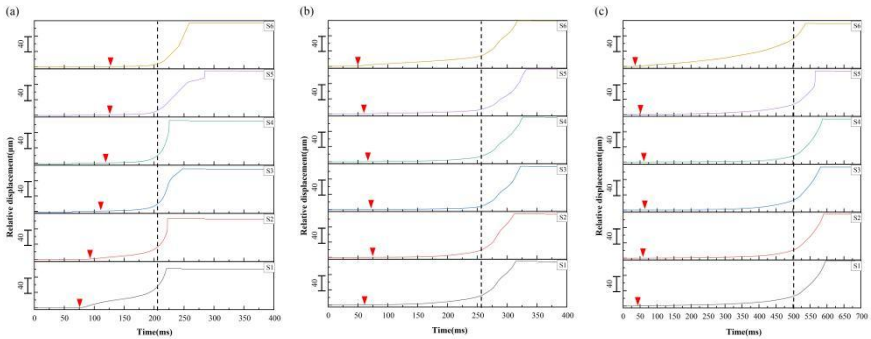


Fig. 6. The displacement curve of each point arranged along the fault over time. (a) Normal stress is 2MPa; (b) Normal stress is 3MPa; (c) Normal stress is 4MPa. (Red triangles and black dashed lines are used in the figure to represent the boundaries of each stage.)

3.3 Directional propagation of bimaterial stick-slip instability fracture

Based on the preceding text, it can be deduced that the initial rupture point is situated in the vicinity of the upper R1 and R6 (or lower R7 and R12). The average velocity of rupture propagation is determined by calculating the spatial distance between adjacent points over time. It is important to note that this velocity does not precisely represent the instantaneous rupture velocity. Observing Fig. 7a and b, an intriguing observation is made where rupture propagation originates from the nucleation region in space and sequentially progresses from left to right at 2MPa. The fracture propagation speed of

the softer material of the upper basalt is slower than that of the harder material of the lower granite, and the fracture occurs earlier.

Moreover, as normal stress increases, fracture propagation manifests in diverse directions, reaching sub-shear velocity (see Fig. 7c and d). This phenomenon occurs because the R6 measurement point in the upper basalt is in close proximity to the fixed end of the loading device, experiencing significant constraints. The heightened normal stress intensifies the constraints at this point, leading to its initial fracture nucleation. Similarly, the lower granite R7, situated near the loading end of the device, experiences pronounced stress concentration, prompting its initial fracture nucleation and forming a dual fracture point.

We refer to the direction of rupture as the positive direction based on the consistent movement direction of softer materials, and vice versa as the propagation in the opposite direction of rupture (see Fig. 7e and f). For the propagation in these two different directions, we analyzed the material stress situation as shown in Fig. 7g. It can be seen that after the stress drop along the fault direction, granite quickly recovers and produces pulse type fracture (slip pulse), while basalt exhibits general crack fracture (sub-shear fracture). The interface slip of the slip pulse can extend to a considerable distance from the fracture tip, and the amplitude is larger, so the destructive power is stronger and the destructive effect is farther. This indicates that any friction will suppress the propagation of slip pulse rupture beyond the limit speed c_{lim} , and there is also a critical rupture speed c_T that causes the material to transition from sub shear failure to slip pulse failure. This is consistent with the study by Shlomai et al^[10-12]. The critical speed c_T related formula is referenced as follows:

$$a_2(c_T)W^2(c_T) - b_2(c_T) = 0 \quad (1)$$

$$\begin{cases} a_n = \sqrt{1 - \frac{c^2}{c_{dn}^2}} \\ b_n = \sqrt{1 - \frac{c^2}{c_{sn}^2}} \\ D_n = 4a_n 4b_n - (1 + b_n^2)^2 \end{cases} \quad (2)$$

$$W(c) = \frac{(1+b_1^2-2a_1b_1)\mu_2D_2 - (1+b_2^2-2a_2b_2)\mu_1D_1}{a_1(1-b_1^2)\mu_2D_2 + a_2(1-b_2^2)\mu_1D_1} \quad (3)$$

Among these, with subscripts, $n=1$ represents softer materials, and $n=2$ represents harder materials. μ_n denotes the Lamé constant, where $E_n(1 + \nu_n)/2$; E_n represents the elastic modulus of the material, and ν_n signifies the corresponding Poisson's ratio. Functions of the rupture velocity c are denoted by $a_n(c)$, $b_n(c)$, $D_n(c)$ and $W(c)$, while c_{dn} represents the longitudinal wave velocity of the material, and c_{sn} stands for the transverse wave velocity of the material. If the fracture propagates in the positive direction, its fracture mode mainly presents two forms: one is crack type fracture, with a fracture speed lower than the critical speed, manifested as sub shear fracture; Another type is pulse rupture, which has a rupture speed higher than and lower than. The negative direction fracture is a crack type fracture, with a sub shear fracture velocity lower than.

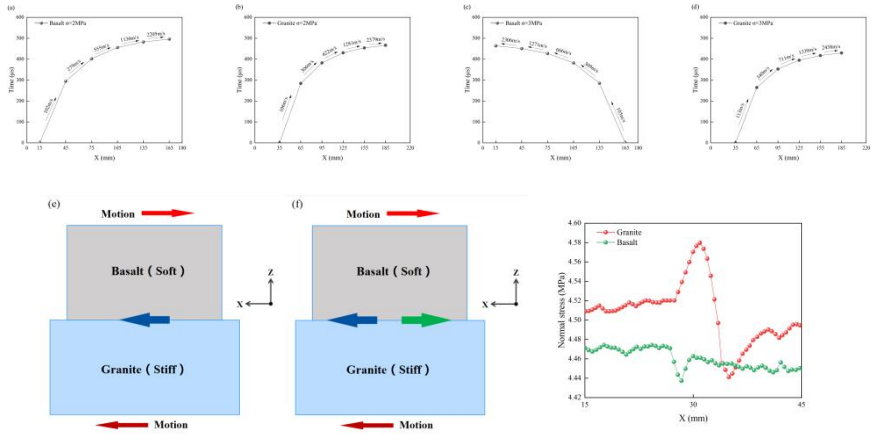


Fig. 7. Spatiotemporal map of fracture propagation in bimaterial faults. (a), (b), (c), (d) Spatiotemporal map of basalt and granite fracture propagation; (e), (f) Schematic diagram of reverse rupture propagation and forward and reverse rupture propagation. (The dark blue arrow represents propagation in the opposite direction, while the green arrow represents propagation in the positive direction.); (g) Schematic diagram of slip pulse rupture and sub shear modes within granite and basalt.

4 Discussion and Conclusion

While we have investigated the stress, displacement, and fracture propagation process associated with bimaterial stick-slip instability and analyzed the mechanism of stick-slip instability from both a global and microscopic standpoint, the lack of material transparency hinders direct observation of the mutual shearing of small particles at the interface. Hence, providing an intuitive display of nucleation positions holds significant research value. Furthermore, this article primarily focuses on strike-slip faults, overlooking the impact of fault thickness. Natural fault structures are intricate and varied, influenced by numerous coupling factors. Nonetheless, this study sheds light on the characteristics of fault nucleation points and fracture propagation direction, offering valuable insights for understanding natural fault instability.

This study investigates the alterations in stick-slip instability of fault systems under varying external conditions through experiments conducted on basalt and granite dual-material fault systems. The research unveils the failure mechanism of stick-slip instability, akin to type II fractures in fracture mechanics. This phenomenon involves the expansion of the initiation point into the nucleation zone, with interconnected nucleation zones leading to instability across the entire cross-section. This process is commonly referred to as the three stages of nucleation within the fracture zone, stable crack development, and dynamic fracture. The specific conclusions drawn from this study are as follows:

(1) There exists a nonlinear positive correlation between normal stress and stress drop. Precursory slip, co-seismic slip, and total slip all escalate with the rise in normal stress, intensifying the fracture propagation process.

(2) A nonlinear negative correlation exists between shear rate and stress drop, as well as the recurrence time of sticky sliding. A critical shear rate marks the transition of instability mode from sticky sliding to stable sliding mode. The longer the interval between recurrences, the more significant the stress reduction. Precursor slip and co-seismic slip decrease with increasing velocity.

(3) In the presence of stick-slip instability on a bimaterial fault, distinct directional characteristics of fracture propagation emerge. When the fracture direction aligns with the sliding direction of softer materials, it is considered a positive fracture direction; otherwise, it is categorized as a negative direction. At low normal stress levels, fracture propagation manifests as sub-shear fractures in the opposite direction. With an increase in normal stress, the fracture propagation is observed to occur in two directions. In the positive direction, a more destructive slip pulse is evident, with a critical velocity c_T marking the transition from sub-shear fracture to slip pulse fracture mode.

Acknowledgement

We are grateful to the National Natural Science Foundation of China (Approval No. 51839009).

References

1. Brace W F. Laboratory studies of stick-slip and their application to earthquakes. *Tectonophysics*, 14(3), 189-200 (1972).
2. Brace WF, byerlee JD. Stick-Slip as a Mechanism for Earthquakes. *Science*, 153(3739): 990-992 (1966).
3. Orowan E. The mechanism of seismic faulting. *Geol. Soc. Am. Mem.*, 79: 232-245 (1960).
4. Matsukawa H, Saito T. Friction, Stick-Slip Motion and Earthquake. *Modelling Critical and Catastrophic Phenomena in Geoscience*, 705, 169-189 (2006).
5. Byerlee J D, Wyss M. Rock Friction and Earthquake Prediction. *Engineering Geology*. 17(4), 286-287 (1978).
6. Dieterich J H. Time-dependent friction and the mechanics of stick-slip. *Pure and Applied Geophysics*, 116(4): 790-806 (1978).
7. Rosakis A J. Intersonic shear cracks and fault ruptures. *Advances in Physics*, 51(4): 1189-1257 (2002).
8. Ruina A. Slip instability and state variable friction laws. *Journal of Geophysical Research Solid Earth*, 88 (1983).
9. Shlomaï H, Fineberg J. The structure of slip-pulses and supershear ruptures driving slip in bimaterial friction. *Nature Communications*, 7, 11787 (2016).
10. Shlomaï H, Kammer D S, Adda-Bedia M, et al. The onset of the frictional motion of dissimilar materials. *Proceedings of the National Academy of Sciences*, 117 (2020).
11. Shlomaï H, M Adda - Bedia, Arias R E, et al. Supershear Frictional Ruptures Along Bimaterial Interfaces. *Journal of Geophysical Research: Solid Earth*, 125 (2020).
12. K. Xia, A. J. Rosakis, H. Kanamori, J. R. Rice, Laboratory earthquakes along inhomogeneous faults: Directionality and supershear. *Science* 308, 681–684 (2005).

13. Zhou, X. P.,Zhang, J. Z.,He, Y..Stick-slip failure in sheared fault with a variety of end constraint degrees: An experimental study[J] *Physics of the Earth and Planetary Interiors*. Elsevier, 301 (2020).

Open Access This chapter is licensed under the terms of the Creative Commons Attribution-NonCommercial 4.0 International License (<http://creativecommons.org/licenses/by-nc/4.0/>), which permits any noncommercial use, sharing, adaptation, distribution and reproduction in any medium or format, as long as you give appropriate credit to the original author(s) and the source, provide a link to the Creative Commons license and indicate if changes were made.

The images or other third party material in this chapter are included in the chapter's Creative Commons license, unless indicated otherwise in a credit line to the material. If material is not included in the chapter's Creative Commons license and your intended use is not permitted by statutory regulation or exceeds the permitted use, you will need to obtain permission directly from the copyright holder.

